

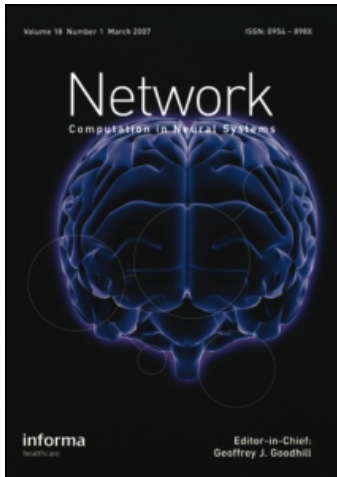
This article was downloaded by: [ETH]

On: 31 May 2010

Access details: Access Details: [subscription number 769797419]

Publisher *Informa Healthcare*

Informa Ltd Registered in England and Wales Registered Number: 1072954 Registered office: Mortimer House, 37-41 Mortimer Street, London W1T 3JH, UK



Network: Computation in Neural Systems

Publication details, including instructions for authors and subscription information:

<http://www.informaworld.com/smpp/title~content=t713663148>

Time and space are complementary encoding dimensions in the moth antennal lobe

Philipp Knüsel^a; Mikael A. Carlsson^{bc}; Bill S. Hansson^{bd}; Tim C. Pearce^e; Paul F. M. J. Verschure^{af}

^a Institute of Neuroinformatics, Zürich, Switzerland ^b Department of Crop Science, Division of Chemical Ecology, SE-230 53 Alnarp, Sweden ^c Astra Zeneca R&D Södertälje, SE-151 85 Södertälje, Sweden ^d Max Planck Institute for Chemical Ecology, Department of Evolutionary Neuroethology, D-7745 Jena, Germany ^e Department of Engineering, University of Leicester, Leicester, LE1 7RH, United Kingdom ^f Technology Department, University Pompeu Fabra, 08003 Barcelona

To cite this Article Knüsel, Philipp , Carlsson, Mikael A. , Hansson, Bill S. , Pearce, Tim C. and Verschure, Paul F. M. J.(2007) 'Time and space are complementary encoding dimensions in the moth antennal lobe', *Network: Computation in Neural Systems*, 18: 1, 35 – 62

To link to this Article: DOI: 10.1080/09548980701242573

URL: <http://dx.doi.org/10.1080/09548980701242573>

PLEASE SCROLL DOWN FOR ARTICLE

Full terms and conditions of use: <http://www.informaworld.com/terms-and-conditions-of-access.pdf>

This article may be used for research, teaching and private study purposes. Any substantial or systematic reproduction, re-distribution, re-selling, loan or sub-licensing, systematic supply or distribution in any form to anyone is expressly forbidden.

The publisher does not give any warranty express or implied or make any representation that the contents will be complete or accurate or up to date. The accuracy of any instructions, formulae and drug doses should be independently verified with primary sources. The publisher shall not be liable for any loss, actions, claims, proceedings, demand or costs or damages whatsoever or howsoever caused arising directly or indirectly in connection with or arising out of the use of this material.

Time and space are complementary encoding dimensions in the moth antennal lobe

PHILIPP KNÜSEL¹, MIKAEL A. CARLSSON^{2,5},
BILL S. HANSSON^{2,6}, TIM C. PEARCE³, &
PAUL F. M. J. VERSCHURE^{1,4}

¹Institute of Neuroinformatics, ETH/University Zürich, Winterthurerstr. 190, CH-8057, Zürich, Switzerland, ²Department of Crop Science, Division of Chemical Ecology, SLU, P.O. Box 44, SE-230 53 Alnarp, Sweden, ³Department of Engineering, University of Leicester, Leicester, LE1 7RH, United Kingdom, ⁴Technology Department, University Pompeu Fabra, Passeig de Circumval·lacio 8, 08003 Barcelona, ⁵Astra Zeneca R&D Södertälje, SE-151 85 Södertälje, Sweden, and ⁶Max Planck Institute for Chemical Ecology, Department of Evolutionary Neuroethology, Hans-Knoell-Strasse 8, D-7745 Jena, Germany

(Received 27 August 2006; revised 23 November 2006; accepted 25 January 2007)

Abstract

The contribution of time to the encoding of information by the nervous system is still controversial. The olfactory system is one of the standard preparations where this issue is empirically investigated. For instance, output neurons of the antennal lobe or the olfactory bulb display odor stimulus induced temporal modulations of their firing rate at a scale of hundreds of milliseconds. The role of these temporal patterns in the encoding of odor stimuli, however, is not yet known. Here, we use optical imaging of the projection neurons of the moth antennal lobe to address this question. First, we present a biophysically derived model that provides an accurate description of the calcium response of projection neurons. On the basis of this model, we subsequently show that the calcium response of the projection neurons displays a stimulus specific temporal structure. Finally, we demonstrate that an encoding scheme that includes this temporal information boosts classification performance by 60% as compared to a purely spatial encoding. Although the putative role of combinatorial spatio-temporal encoding strategies has been the subject of debate, our results for the first time establish quantitatively that such an encoding strategy is used by the insect brain.

Keywords: *Functional imaging, olfaction, neuronal coding*

Correspondence: Philipp Knüsel, Institute of Neuroinformatics, ETH/University Zürich, Winterthurerstr. 190, CH-8057, Zürich, Switzerland. Tel: +41 44 635 3072. Fax: +41 44 635 3053. E-mail: pknuesel@web.de

Introduction

The role of time in the encoding of information by the nervous system has been debated for decades (deCharms and Zador 2000). In this debate, a distinction is usually made between population and single cell encoding. At the level of neuronal populations, it has been argued, going back to Milner (1974), that synchronous neuronal activity could provide the substrate to functionally link information encoded in spatially distributed activity patterns and therefore solve the, so called, binding problem (Milner 1974; von der Malsburg 1981; Singer and Gray 1995). Synchrony has been observed in a number of neuronal systems (Ritz and Sejnowski 1997) including the olfactory system where output neurons of the antennal lobe or the olfactory bulb have been reported to display sequences of synchronized assembly responses to odor stimulation (Laurent 2002). At the level of single neurons, evidence from various sensory systems suggests that neurons can also show temporally patterned responses to static sensory stimuli (McClurkin et al. 1991; Middlebrooks et al. 1994; Katz et al. 2001; Panzeri et al. 2001; Laurent 2002; Di Lorenzo and Victor 2003). In the olfactory system, the output neurons of the antennal lobe/olfactory bulb display temporally patterned responses at a time scale of hundreds of milliseconds (Friedrich and Laurent 2001; Laurent 2002). Previously, we and others have shown that this temporal patterning is accompanied by a decrease of the similarity between spatial odor representations in the antennal lobe/olfactory bulb with time (Friedrich and Laurent 2001; Carlsson et al. 2005). Despite elaborate considerations on the putative role of these temporal patterns in neuronal processing (Laurent 2002) and experimental data suggesting that their structure depends on the stimulus (Friedrich and Laurent 2004), the information content of these temporal patterns in the encoding of odor stimuli has so far not been quantified. In the context of the olfactory system, both of the aforementioned properties of projection neuron/mitral cell response, i.e., synchronization and temporal patterning, have been referred to as “temporal coding”. It is important to emphasize that we only deal with the latter in this study. In particular, we assess and quantify here the information content of the temporal patterns of projection neuron activity in the encoding of odor stimuli. This study is in this context the first that does not only argue for a role of time in neuronal encoding but quantifies this contribution for the antennal lobe system of the moth. In earlier theoretical investigations of the encoding and decoding of static stimuli into temporal patterns of neuronal activity by a so-called temporal population code (Wyss et al. 2003a, 2003b; Knüsel et al. 2004), we have shown that the temporal structure of the summed activity of a laterally coupled neuronal population can provide for a robust and rapid encoding of static stimulus features. The current study was developed to empirically validate our hypothesis that the temporal structure of neuronal activity contains information about static stimuli.

We quantify and assess the accuracy and the speed of the encoding of odor stimuli by the antennal lobe based on spatial, temporal, and spatio-temporal encoding schemes, using optical imaging derived from the projection neurons of the moth antennal lobe (Carlsson et al. 2005). Whereas optical imaging analysis methods usually focus on extracting spatial activation patterns (Frostig 2002; Sornborger et al. 2003), here, we propose a model-based analysis method that also allows for a precise quantification of the temporal dynamics of the optical response. The optical response we analyze is measured in the center of the glomeruli visible in the staining

of the antennal lobe and visualizes the integrated inputs of the projection neurons leaving the antennal lobe via the inner antenno-cerebral tract (Carlsson et al. 2005). As most projection neurons of that tract are uniglomerular (Anton and Homberg 1999), we call this response the optical projection neuron response of a glomerulus (or, the optical projection neuron response). We fit (Stetter et al. 2001) a biophysically derived model function (Neher and Augustine 1992; Helmchen et al. 1996; Yasuda et al. 2004), a so-called alpha function, to the optical projection neuron response. On the basis of this model, we quantitatively assess first to what extent the temporal pattern of the optical projection neuron response is modulated by odor stimuli and subsequently which properties of this response contain information on odor stimuli. We show that the spatial and temporal components of the optical projection neuron response to odor stimuli are uncorrelated and that a combinatorial spatio-temporal encoding of odor stimuli renders a 60% improvement in odor classification as compared to a purely spatial encoding scheme. Hence, our results confirm our earlier prediction, and prove that the temporal dynamics of neuronal activity, measured on a time scale of hundreds of milliseconds, contains a significant amount of information about sensory stimuli.

Methods

Preparation of animals

Preparation of animals, dye loading, optical recordings, and odor delivery are identical to Carlsson et al. (2005). Male *Spodoptera littoralis* were used 2–4 days post-eclosion. The animals have been reared for several generations on a potato-based diet (Hinks and Byers 1976). The pupae were separated according to sex and kept in plastic boxes at 70% relative humidity, 23°C and a 16 h/8 h light/dark cycle. Adult moths were supplied with water ad libitum until the start of experiment.

Animals were restrained in plastic pipette tips, with only the heads protruding. Dental wax was used to secure the animal in the holder and to minimize movements. The brain of the moth was uncovered by opening up a window in the cuticle between the compound eyes and by removing muscles, glands, and tracheae. Mouthparts and proboscis were also removed. The brain was superfused with moth saline (Christensen and Hildebrand 1987).

Dye loading

Retrograde selective staining of projection neurons through the inner antenno-cerebral tract was performed by injection of a dye-coated glass electrode (tip diameter 10–20 µm) into the inner antenno-cerebral tract. The majority of uniglomerular projection neurons leaving the antennal lobe have been shown to exit through the inner antenno-cerebral tract in *S. littoralis* (Anton and Hansson 1994, 1995; Sadek et al. 2002), and about five to six projection neurons of the inner antenno-cerebral tract innervate a single glomerulus (Anton and Homberg 1999). Crystals of FURA-dextran (10000 MW, Molecular Probes, Eugene, USA) were dissolved in a 2 ml bovine serum albumin (~5% solution) and the tip of the electrodes was coated with the dye. The level of the moth saline was temporarily

lowered to prevent the dye from dissolving prior to injection in the brain. To aim for the inner antenno-cerebral tract the electrode was manually inserted close to the midline of the brain about halfway between the antennal lobe and the mushroom bodies. The dye was allowed to diffuse for 10–20 s before the electrode was removed. After rinsing with moth saline the preparation was incubated in a cold (8–12°C) and dark chamber for about 3 h. This procedure results in a staining of the antennal lobe as well as the inner antenno-cerebral tract (Carlsson et al. 2005). The optical responses are odor dependent and reproducible with repeated stimulations both within and between animals (Carlsson et al. 2005).

Optical recordings

We used a TILL Photonics air-cooled imaging system (Gräfelfing, Germany) with a 12 bit slow-scan CCD camera. Filter settings were dichroic: 410 nm; emission LP 440 nm and the preparation was alternately excited at 340 and 380 nm. Exposure times were ~20 and 60 ms, respectively. Sequences of 70 double frames at a sampling rate of 10 Hz were recorded through an upright Olympus microscope with a 20× (NA 0.50; Olympus, Japan) water immersion objective. On-chip binning (2 × 2) was performed, which resulted in a final image size of 320 × 240 pixels. The pixel size at 20× magnification corresponded to ~1 × 1 μm². Execution of protocols was made using Till-vision 4.0 (TILL Photonics).

Odor delivery

A moistened and charcoal filtered continuous air stream (30 ml s⁻¹) was ventilating the antenna ipsilateral to the recorded antennal lobe through a glass tube (7 mm ID). The glass tube ended ~10 mm from the antenna. An empty Pasteur pipette attached to a plastic pipette tip (volume ~4.5 ml) was inserted through a small hole in the glass tube, blowing an air stream of about 5 ml s⁻¹. Another air stream (~5 ml s⁻¹) was blown through the odor-loaded pipette by a computer-triggered puffer device (Syntech, The Netherlands) during 1 s (started at frame 20) into the continuous stream of air. During stimulation the air stream was switched from the empty pipette to the odor-loaded one, in order to minimize the influence of mechanical stimulation.

In six animals, we used the odors 1-octanol, geraniol, (+/-)-linalool and phenylacetaldehyde (PAA) at doses of 50 μg and 100 μg (except one animal where only 1-octanol and PAA at both doses were tested). In a seventh animal, additionally benzaldehyde, eugenol, E2-hexenal, and heptanol were used (all eight odors at 50 μg, heptanol at 17 μg (Meijerink et al. 2003)). The odorants used are biologically relevant to the animal as components of green leaves and flowers of host-plants or emitted from larval frass (Anderson et al. 1993; Jönsson and Anderson 1999). The purity of the compounds was between 95 and 99% and they were dissolved in paraffin oil. Ten microlitre of the solvent containing 50 μg of the respective odorant were applied on filter papers (5 × 15 mm²). The filter papers were inserted in Pasteur pipettes, attached to plastic pipette tips, sealed with Para-film (American National Can., Chicago, USA) and stored in a freezer (-20°C) until the start of an experiment. Control stimuli consisted of filter paper with solvent (10 μl) only.

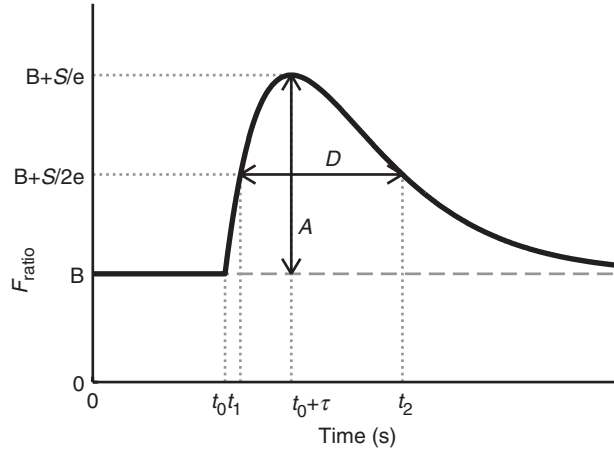


Figure 1. Alpha-function. The four parameters of the alpha function are the amplitude-coefficient S , the baseline shift B , the response onset t_0 , and the decay time constant τ . The amplitude, A , is the difference between the peak and baseline activity of the alpha function, and the duration, D , is the width of the alpha function at half maximum limited by t_1 and t_2 .

Odorants and control were delivered in a randomized order. Each odor was presented between 1 to 12 times, and we allowed at least 60 s between stimulations to reduce adaptation effects.

Optical projection neuron response and its model

The optical projection neuron response is the bleaching corrected luminance measured from the center of the glomeruli of the antennal lobe. We have fitted this response with a biophysical model that essentially comprises an alpha function (Figure 1 and Appendix A).

$$\alpha(t; S, B, \tau, t_0) = B + \begin{cases} 0 & \text{if } t < t_0 \\ S \frac{t - t_0}{\tau} \exp\left(-\frac{t - t_0}{\tau}\right) & \text{else} \end{cases} \quad (1)$$

The four parameters of the alpha function, the amplitude-coefficient, S , the baseline, B , the time constant, τ , and the response onset, t_0 , are found with, for example, nonlinear regression. Following this approach we extract from the fitted alpha function the response amplitude, A , and duration, D , of the optical projection neuron response. We perform our further quantification of the information content of the optical projection neuron response using these two measures. Appendix A and B provide detailed descriptions of data preparation, the biophysical model, the derivation of the alpha function model, its fit to the optical projection neuron response and the further statistical procedures we have used.

Data analysis

Data analysis is done using Matlab (The MathWorks, Inc., Natick, MA, USA) and SPSS (SPSS, Inc., Chicago, IL, USA). For analysis of variance (ANOVA),

independent variables (factors) are either the glomerulus, the odor stimulus, or odor identity and odor concentration. In case of glomeruli, ANOVAs are performed for each animal individually to prevent use of possibly repeatedly sampled glomeruli as independent variables. Dependent variables are either response amplitude or duration. The dependent variables are weighted with the inverse square of their standard deviation in order to correct for different accuracies in their estimates. The significance level is always $\alpha = 0.05$. In case of 2-way ANOVAs, the result is discarded if a significant interaction is detected.

The effect sizes of the two factors odor identity and concentration are measured using eta squared, η^2 . This measure is defined as

$$\eta^2 = \frac{S_{\text{effect}}^2}{S_{\text{total}}^2} \quad (2)$$

with S_{effect}^2 the weighted sum of squares of the effect (odor identity or concentration), and S_{total}^2 the total weighted sum of squares. η^2 thus measures the fraction of total variability that is accounted for by each factor.

Predictive linear discriminant analysis (LDA) is used to predict the identity and concentration of an odor sample. We assess the fraction of correct classifications, i.e., the ratio of correctly classified samples vs. the total number of samples, with a so-called leave-one-out test. In this test, each sample is left out once and classified based on the discriminant functions derived from all remaining samples. Note that for this test we exclusively use LDA as a linear transformation of the representation of odors from one space to another, without computing any p -values. Thus, testing the assumptions of LDA is not required.

In the classification analyses, each glomerulus represents the odor stimuli by means of either one of two response parameters or their combination. Missing values of the response parameters are replaced with the corresponding mean. We assess the fraction of correct classifications using the response parameters of subsets of glomeruli. As any read-out process is solely dependent on the information available in a single animal, these subsets of glomeruli are formed for each animal individually. The maximally possible size of these subsets depends on the number of samples and is between three and seven (six animals). The number of variables for the LDA corresponds either to the size or the doubled size of the subsets of glomeruli (dependent on whether only one or both response parameters represent the odor stimuli). In order to exclude those subsets of glomeruli that provide an insufficient encoding of the odor stimuli, we use for each size of the subsets only those 50 for which the fraction of correct classifications using the combined response parameters is best. The six animals used for the classification analyses are stimulated with eight odors except one where only four odors are tested and another one where more than one repetition is acquired to five odors. In order to correct for the different number of odor stimuli, fraction correct values are weighted with the according number of odor stimuli divided by the mean number of stimuli. Of these values, the median and the standard error of the median is computed. Tests showed that using unweighted fraction correct values yields similar results.

We carry out two classification analyses. In a first analysis, odor samples are represented using an encoding based on the response amplitude, duration, or their combination (i.e., a combinatorial encoding). The second analysis is based on instantaneous counterparts of these encoding schemes where either the

instantaneous amplitude of the model function, its derivative (i.e., the instantaneous amplitude change), or their combination represent the odor.

The fraction correct values of the different encoding schemes are statistically compared using Friedman's test ($\alpha=0.05$). Post-hoc pair-wise comparisons are performed using Wilcoxon's rank sum test. We use the Dunn–Sidak correction to adjust the significance level for the individual comparisons such that the significance level for the complete set of comparisons is $\alpha_E=0.05$. The corrected significance level is given by $\alpha = 1 - (1 - \alpha_E)^{(1/N)}$ where N is the number of comparisons.

Results

We will start by describing the fit of our alpha function model to the optical projection neuron response. Subsequently we will assess to what extent its characteristic parameters, amplitude, and duration, can be considered viable encoding dimensions.

Optical projection neuron response and fit validation

We first illustrate the basic properties of the optical projection neuron response. We observe that odor stimulation of the animal results in a fast increase of the intracellular calcium concentration of projection neurons within 0.2–0.3 s (Figure 2b and c, dotted lines). This increase is followed by a slow decay back to baseline.

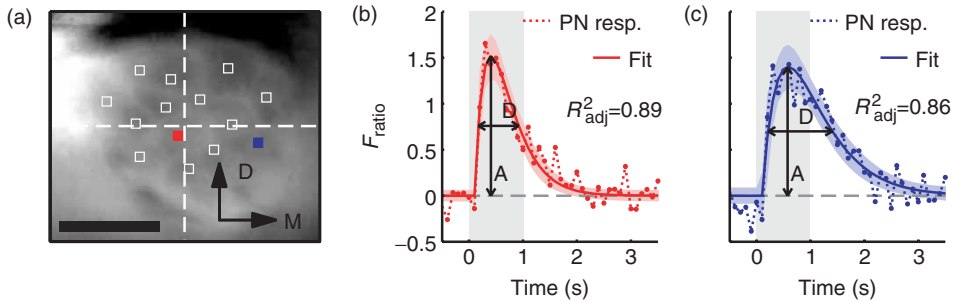


Figure 2. Morphological view of the antennal lobe and time courses to stimulation with PAA at 100 μg during 1 s. (a) Morphological view of the antennal lobe after staining with FURA-dextran through the inner antenno-cerebral tract. Note that the borders of the glomeruli are visible. These borders are used to position the sampling rectangles (white and colored squares) in the centers of the glomeruli. The sampling rectangles are used to compute the time course of the optical projection neuron response. The red and blue squares correspond to the time courses of panel (b) and (c), respectively. Scale bar: 100 μm , D: dorsal, M: medial. (b, c) Time courses of the optical projection neuron response of two glomeruli (dotted line, larger dots indicate actual samples) including the fitted model function, an alpha function (solid line, see “Methods” and Appendix A), and simultaneous prediction bounds (shaded area) (Seber and Wild 1989). The two black lines with arrow heads indicate the response amplitude (A) and the response duration (D). The light-grey bar indicates the stimulus, the grey dashed line indicates baseline activity. R^2_{adj} is the value of the adjusted R^2 statistic (Appendix B).

The fit of our model to the optical projection neuron response shows that the projection neuron calcium dynamics induced by odor stimulation is well characterized by an alpha function (Figure 2b and c, solid lines). This is further confirmed by an adjusted R^2 -squared statistic of the fit, R_{adj}^2 , close to 1 (Appendix B). Additional detailed graphical and analytical analyses of the goodness of the fits showed that alpha functions provide a precise representation of the optical projection neuron response in 85% of all cases (Appendix B). Hence, the optical projection neuron response can be accurately described in terms of amplitude and duration.

The optical projection neuron response displays a stimulus specific temporal structure

A necessary condition for an encoding scheme that incorporates both the amplitude and the duration of the optical projection neuron response of a glomerulus is that different glomeruli should display distinct values for these response parameters. This condition is satisfied by the majority of our sample: seven animals for the response amplitude and five for the response duration (total of seven animals, weighted 1-way analyses of variance (ANOVAs), factor: glomerulus, between 12 and 18 glomeruli per animal, median p -value for amplitude: $\langle p \rangle \approx 5.7 \times 10^{-22***}$, median p -value for duration: $\langle p \rangle \approx 0.002**$). Hence, this shows that the amplitude-time course of the optical projection neuron response to an odor stimulus is different between glomeruli.

A second condition for an encoding scheme that takes into account both the amplitude and the duration of the optical projection neuron response of a glomerulus is that different odor stimuli should evoke distinct values for these response parameters. Indeed, pooled across all glomeruli of all animals (seven animals, 78 glomeruli), we find that odor stimuli have a significant effect on both the response amplitude and duration (weighted 1-way ANOVAs, factor: odor stimulus, amplitude: $F(11, 1703) \approx 5.7$, $p \approx 3.7 \times 10^{-9***}$, duration: $F(11, 1703) \approx 65.6$, $p << 0.001***$). When we analyze the data at the level of single glomeruli, we observe that 26 glomeruli show significant simultaneous modulations of both amplitude and duration, while 21 display modulations of only the duration and 6 show modulations of only the amplitude (weighted 1-way ANOVAs, factor: odor stimulus, $\alpha = 0.05$, median of p -values for simultaneous modulation: $\langle p \rangle \approx 2.6 \times 10^{-4}$, only duration: $\langle p \rangle \approx 0.007$, only amplitude: $\langle p \rangle \approx 0.002$). Thus, response amplitude and duration of most glomeruli are modulated in a combinatorial manner.

A third condition for an encoding scheme that is based on the amplitude and the duration of the optical projection neuron response of a glomerulus is that these response parameters should be linearly independent. The distribution of the response duration and amplitude of two arbitrary glomeruli shows that the response parameters to different odor stimuli are indeed clustered and are not significantly correlated (Figure 3a–c). Across all glomeruli, we observe that amplitude and duration show an arbitrary correlation structure and are almost as often negatively correlated as positively (Figure 3d). Moreover, in 59 out of 78 glomeruli, the observed correlation is statistically not significant ($\alpha = 0.05$). Thus, amplitude and duration of most glomeruli are linearly independent.

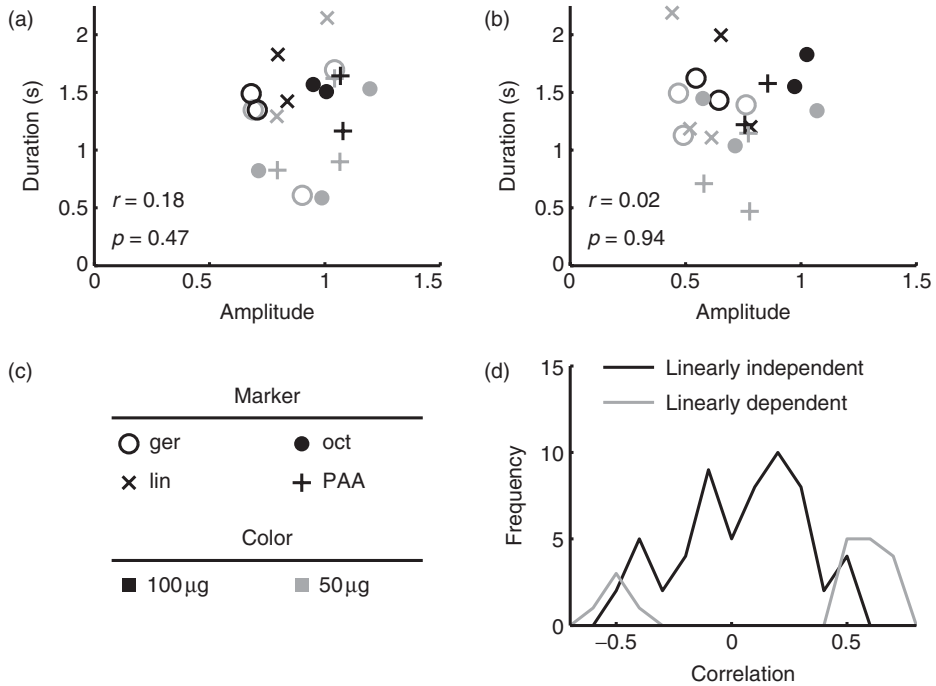


Figure 3. Correlation between response duration and amplitude. (a, b) Response duration vs. amplitude for two glomeruli showing no significant correlation between amplitude and duration. The correlation, r , and its p -value, p , are given in the figure. (c) Legend for panels (a) and (b). (d) Distribution of correlation coefficients for all glomeruli. Statistically not significant correlations indicate that amplitude and duration are linearly independent (black), while significant correlations indicate a linear dependence (gray). Abbreviations: geraniol (ger), linalool (lin), octanol (oct), phenylacetaldehyde (PAA).

In summary, these results show that for a majority of the glomeruli amplitude and duration of the optical projection neuron response are uncorrelated and significantly modulated by odor stimuli in a combinatorial manner. Thus, similar to the temporal patterning of the projection neuron's or the vertebrate's mitral cell's firing rate (Friedrich and Laurent 2001; Laurent 2002; Stopfer et al. 2003; Friedrich and Laurent 2004), the optical projection neuron response of most glomeruli displays a stimulus specific temporal structure.

Contribution of stimulus to modulation

So far we have demonstrated that odor stimuli can induce significant modulations of the duration and amplitude of the optical projection neuron response. To exclude the trivial result that this modulation can be accounted for by the concentration itself, i.e., a higher concentration could boost the amplitude or the duration of the response, we assess the individual effect sizes of odor identity and concentration using eta squared, η^2 ("Methods"). We observe that the effect size of the odor identity on both the amplitude and the duration of the optical projection neuron

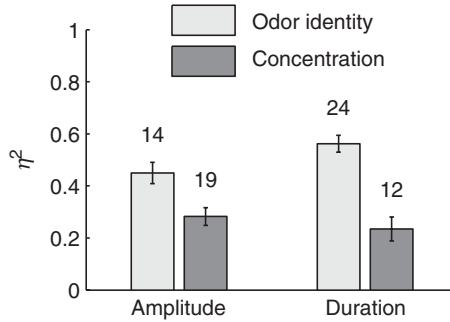


Figure 4. Mean effect size (η^2 , see “Methods”). η^2 is averaged for all four combinations of odor identity/concentration with amplitude/duration. In the computation of the pooled averages, only effect sizes are used for which a significant p -value was returned by the weighted two-way ANOVAs of the amplitude and duration of the optical projection neuron response of each individual glomerulus (factors for ANOVA: odor identity and odor concentration, number of corresponding glomeruli that displayed significant effects given above each bar). Error bars indicate the standard error of the mean.

response is about twice as large as that for concentration. Moreover, each of these stimulus properties has a practically constant effect on the response parameters (Figure 4, 2-way ANOVA of η^2 , six animals, total of 65 glomeruli, amplitude/duration: $F(1, 65) \approx 0.7$, $p \approx 0.41$, odor/concentration: $F(1, 65) \approx 40.7$, $p \approx 2.1 \times 10^{-8***}$, interaction: $F(1, 65) \approx 4.3$, $p \approx 0.043^*$). Thus, the modulation of the response duration by an odor stimulus is as strong as that of the amplitude and most of this modulation is accounted for by the identity of an odor.

Encoding of odor stimuli

Since both the amplitude and the duration of the optical projection neuron response depend on the odor stimulus, we want to assess to what extent these two response parameters contain information on odor stimuli. We compute for subsets of glomeruli the fraction of correct odor classifications using three encoding schemes: an encoding based on amplitudes, an encoding based on durations, and an encoding based on their combination, i.e., combinatorial encoding (Figure 5 and “Methods”, six animals). We find that the average fraction of correct classifications for the combinatorial encoding is significantly higher than for the two non-combinatorial encodings for subset sizes larger than one (Friedman’s test for each subset size, between 85 and 300 data points per condition, $p \ll 0.001$ for all sizes; post-hoc Wilcoxon rank sum tests of all pair-wise comparisons for a fixed subset size, $\alpha = 0.017$ corrected for three consecutive comparisons, $p > \alpha$ for subset size one, but $p \ll 0.001$ for all other subset sizes, see “Methods”). Moreover, we observe that an increased subset size contributes an additional and significant amount of information as expressed in fraction of correct classifications (Wilcoxon’s rank sum tests for each encoding scheme between consecutive subset sizes, $p \ll 0.001$ for all comparisons). Thus, the encoding of odor stimuli into the amplitude and the duration of the optical projection neuron response is complementary; their

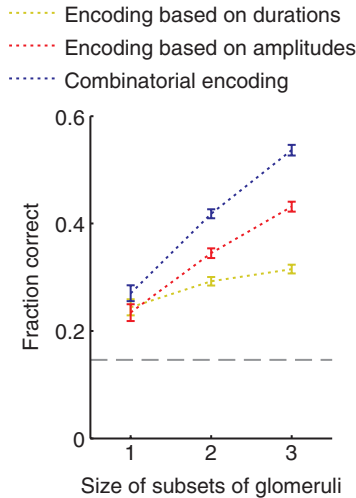


Figure 5. Median fraction of correct classifications vs. the size of subsets of glomeruli. For each subset of glomeruli, odor stimuli are represented by either the according response durations, response amplitudes, or their combination (yellow, red, and blue line, respectively). The odor stimuli are classified with predictive LDA, and the fraction of correct classifications is computed with a so-called leave-one-out test (“Methods”). Error bars indicate the standard error of the median. The dashed grey line indicates chance level. $n = 6$ animals.

combination yields a higher information content than each of these components in isolation.

An important issue in the encoding of odor stimuli into the combination of the amplitude and the duration of the optical projection neuron response is how rapidly the encoded information is available without having to compute the actual response duration which would require integration over hundreds of milliseconds. To investigate this question we use the alpha function model to replace the amplitude and duration of the optical projection neuron response with their instantaneous counterparts, i.e., the instantaneous amplitude of the model function and its temporal derivative, the instantaneous amplitude change. The three instantaneous encoding schemes we investigate are the encoding based on instantaneous amplitudes, instantaneous amplitude changes, and their combination, the instantaneous combinatorial encoding. For each of these encoding schemes, we compute the time course of the fraction of correct classifications for maximally sized subsets of glomeruli (six animals, “Methods”). This reveals that the peak classification performance of the instantaneous combinatorial encoding scheme and the instantaneous amplitude encoding method is reached at about 0.8 s and 0.9 s after stimulus onset, respectively (Figure 6a). This time is significantly earlier compared to the peak performance of the instantaneous amplitude change encoding reached at 1.5 s (Friedman’s test, $p \ll 0.001$, $n = 300$ data points per condition, post-hoc Wilcoxon rank sum tests with corrected $\alpha = 0.017$). Excluding the latency of about 0.1–0.2 s due to the odor delivery system (Anton and Hansson 1994), peak classification performance of the instantaneous combinatorial encoding is reached at about 0.6–0.7 s after stimulus onset. Interestingly enough, the time of the performance peak lies well within the stimulation period. In summary, with respect

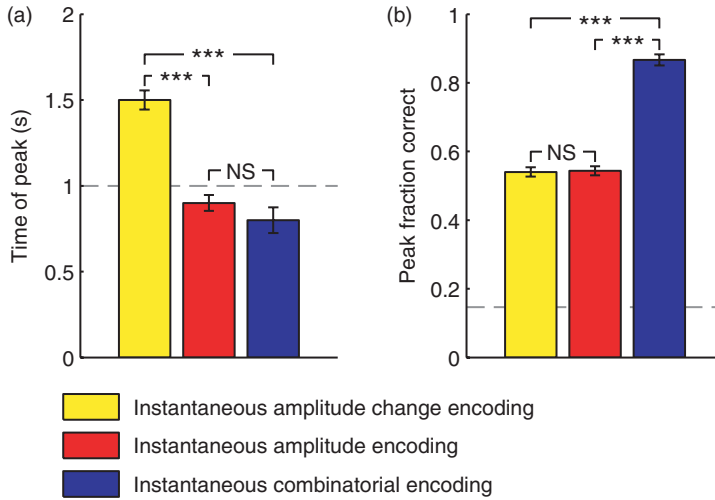


Figure 6. Speed and accuracy of odor discrimination for subsets of glomeruli. The instantaneous dynamics of the alpha functions fitted to the optical projection neuron responses are defined by their instantaneous amplitudes and derivatives, i.e., the instantaneous amplitude changes. At each point in time, these measures are used to classify stimuli with predictive LDA using a leave-one-out test to determine the fraction of correct classifications (“Methods”). The time course of the fraction correct is computed for an encoding based on either the instantaneous amplitude change, the instantaneous amplitude, or their combination. Based on these time courses, (a) the average time of the peak and (b) the peak fraction correct are computed. The time in (a) is relative to stimulus onset, and the dashed line indicates stimulus offset. The dashed line in (b) indicates the chance level. The values shown are the median plus/minus the standard error of the median ($n = 6$ animals, see “Methods”). The medians are tested for significant differences (Wilcoxon’s rank sum test, significance levels: $p < 0.001$ (***) , not significant (NS), $\alpha = 0.017$, see text).

to encoding latency the instantaneous combinatorial encoding is at least as fast as the instantaneous amplitude encoding and faster than the instantaneous amplitude change encoding.

Finally, we want to assess the accuracy of the instantaneous encoding schemes. We compute the peak fraction of correct classifications using the time course of the fraction correct values described earlier. We observe that the instantaneous combinatorial encoding yields a significantly higher fraction of correct classifications with a maximum of about 87% compared to 54% for the instantaneous amplitude and amplitude change encodings (Friedman’s test, $p \ll 0.001$, $n = 300$ data points per condition, post-hoc Wilcoxon rank sum tests with corrected $\alpha = 0.017$, see Figure 6b). Thus, combining a purely spatial encoding based on a vector of instantaneous response amplitudes with information about the temporal structure, as provided by the change of the instantaneous response amplitudes leads to an about 60% boost in the accuracy of the encoding.

Relation between optical response of projection neurons and their firing rate

The signal we analyzed, i.e., the optical projection neuron response, is the intracellular calcium concentration of projection neurons as measured from

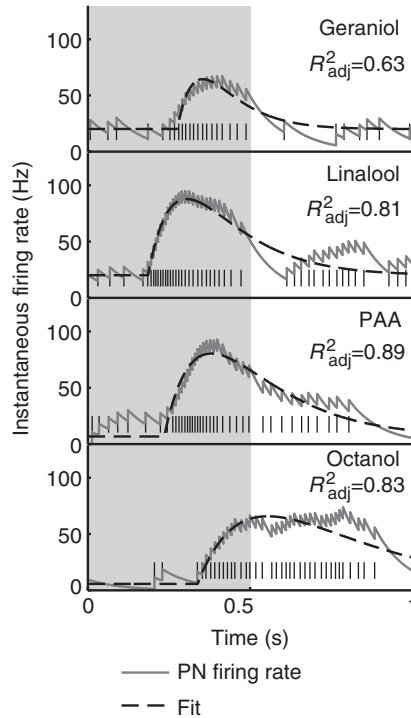


Figure 7. Alpha functions fitted to the projection neuron firing rate. The instantaneous firing rate (gray line) and spikes (vertical lines) of four projection neurons, measured in different animals, is shown. The firing rate was computed by convolving the spike train with an exponential decay ($\tau = 100$ ms). Alpha functions (black dashed lines) were fitted to the firing rate. The shaded area indicates the stimulus, and R^2_{adj} is the value of the adjusted R^2 statistic (“Methods”).

the glomeruli. Each glomerulus is innervated by about five to six projection neurons of the inner antenno-cerebral tract (“Methods”) (Anton and Homberg 1999). We showed that this optical signal can be accurately described by an alpha function. Following this approach we demonstrated that the temporal structure of the optical projection neuron response carries significant additional stimulus specific information. Hence, this raises the important question of how the projection neuron firing rate relates to the optical projection neuron response. Previous studies of single projection neurons and mitral cells suggested that their intracellular calcium concentration can correspond to their spiking activity (Charpak et al. 2001; Galizia and Kimmerle 2004). In this case, and since the *measured* calcium concentration, i.e., the optical projection neuron response, is the convolution of the “true” intracellular calcium concentration with an exponential decay (Appendix A), the optical projection neuron response can be best approximated by a spike train that is convolved with an exponential decay. Indeed, when we inspect electrophysiological recordings of moth projection neurons, we observe that the convolution of the spikes with an exponential decay, the firing rate, is well represented by an alpha function during the stimulation period (Figure 7). Hence, the firing rate of the projection neurons and their optical signal may be connected with each other via

a convolution with an exponential decay. More support for this hypothesis comes from a recent study of Friedrich, where the opposite direction was taken (Yaksi and Friedrich 2006): It was shown that firing rate changes could be computed by deconvolving the time course of the optically recorded calcium signal with an exponential decay. Thus, this suggests that the observed calcium dynamics reflect the electrical projection neuron response dynamics during stimulus presentation.

Discussion

We have investigated the role of the time in the encoding of sensory stimuli. In particular we have shown that the optical projection neuron response to odor stimuli can be described by an alpha function based biophysical model. Using this approach we have demonstrated that the optical projection neuron response can be characterized with only two parameters, amplitude and duration. Our analysis revealed that the amplitude and duration of the optical projection neuron response are uncorrelated and significantly modulated by the identity and concentration of the odor stimuli. Thus, the optical projection neuron response displays a temporal patterning that is stimulus specific. When we combined a spatial encoding scheme with information on the temporal structure of the optical projection neuron response, we observed a classification performance boost of 60%.

The imaged optical projection neuron responses in the moth antennal lobe combine the activity of about five to six projection neurons (Anton and Hansson 1994). Electrophysiological recordings of single projection neurons showed that they can respond with complex temporal patterns to odor stimulation (Anton and Hansson 1994, 1995; Friedrich and Laurent 2001; Laurent 2002; Sadek et al. 2002; Stopfer et al. 2003; Friedrich and Laurent 2004). These patterns can differ between neurons for the same stimulus and for the same neuron between stimuli. Hence, the single alpha function deployed here to quantify the information content of the optical projection neuron response is likely to underestimate the information content of the projection neuron responses. It is thus important to emphasize that our results provide a lower bound for the information content of the optical projection neurons responses, suggesting that the actual information that the temporal structure of a projection neuron response conveys is actually higher than the one identified here. This, however, only emphasizes the relevance of our observation.

In our experiments, we measured the optical projection neuron response to make inferences on the information processing by the antennal lobe, that is, we use the intracellular calcium concentration of the projection neurons, measured in the glomeruli, as a probe of the dynamics of the antennal lobe network. Our analysis showed that this network, i.e., the conglomerate of olfactory receptor neurons, local neurons, projection neurons, and modulatory projections (Anton and Homberg 1999), transforms the receptor response to odor stimuli into a representation where both the instantaneous amplitude and the derivative of the calcium response of projection neurons contain significant odor information. In order to assess whether these two features are part of the actual code employed by the projection neurons, we need to determine whether they are *transduced* by projection neurons and *decoded* by downstream neurons.

While the decoding question lies beyond the scope of this article we can address the transduction question, i.e., whether – as suggested by our results – the projection neuron firing rate and its derivative *contain* odor information. We already presented evidence that the measured calcium dynamics reflect the underlying electrical projection neuron response dynamics. In that case, and because we showed in this article that there exists odor information in the instantaneous amplitude of the optical signal, our results suggest that also the projection neuron firing rate contains odor information. Indeed, there is ample evidence supporting this notion (Friedrich and Laurent 2001; Stopfer et al. 2003; Friedrich and Laurent 2004; Mazor and Laurent 2005). In addition, we demonstrated in this article that odor information is also encoded in the derivative of the optical signal. Hence, this suggests that also the derivative of the projection neuron firing rate contains information about odor stimuli. However, this hypothesis has to the best of our knowledge not yet been addressed and future work will need to evaluate this prediction.

The previously reported temporal pattern of projection neuron or mitral cell responses to odor stimulation is different from the one found here. Locust projection neurons or zebrafish mitral cells, for instance, can respond with complex temporal patterns of increasing and decreasing firing rates to odors (Friedrich and Laurent 2001; Laurent 2002; Friedrich and Laurent 2004; Brown et al. 2005; Mazor and Laurent 2005). In contrast, the optical projection neuron response analyzed here is much less complex. The time course of the optical signal we analyzed in this study could be sufficiently characterized by a fast increase of calcium concentration followed by a slow exponential decay, i.e., an alpha function.

Before discussing potential explanations for these differences, we first address the relation between calcium concentration and electrical activity. In general, this relation is subject to an ongoing debate. It has been suggested that calcium concentration can correspond to spiking activity of projection neurons or mitral cells (Charpak et al. 2001; Galizia and Kimmerle 2004) and that firing rate changes can be computed by deconvolving the time course of the optically recorded calcium signal (Yaksi and Friedrich 2006). However, despite these suggestions that calcium activity can correspond to electrical activity, the literature disagrees on the exact extent of this correspondence. Galizia and Kimmerle (2004), for instance, emphasized that optically recorded projection neurons could display broader response profiles compared to the electrophysiologically recorded response of the same neuron. A potential explanation for this difference is that the measurement of calcium concentration was performed in dendritic compartments and thus potentially far away from the spike initiating zone of the neuron. Thus, the difference between electrical and optical signal could be accounted for by dendritic processes such as leak and/or inhibition of the neuron close to the spike initiating zone which may not be visible in the optical signal.

A similar explanation could account for the differences in complexity of the temporal pattern of the projection neuron response we analyzed here compared to other species. Because we recorded projection neuron calcium concentration in the center of the glomeruli, our recordings may be primarily dominated by calcium influx controlled by olfactory receptor neurons. In other words, the optical projection neuron response is derived from compartments of the cell that are not subject to integration of inputs from local neurons and thus underly a less pronounced temporal modulation than electrophysiological recordings of

projection neurons. Hence, the optical recording technique itself could in part account for the different complexity of the temporal pattern of the projection neuron response. Thus, although we can safely predict that the temporal modulation of the optical projection neuron response will be transduced into firing activity the details of this transduction process demand further electrophysiological investigation.

The goal of this article was to assess as an external observer the information content that lies in the temporal dynamics of the optical projection neuron response. This way of “decoding by observers” is distinct from the question of how a biological system does the actual decoding in one crucial aspect: While “decoding by observers” permits us to employ any possible technique to extract all useful information from a data set, the latter question requires the decoding process to be biologically realistic and thus prohibits many of the possible analysis techniques. In order to allow a fair comparison between possible decoding approaches, we list in the following the techniques that a biological substrate is likely not to have access to and that therefore could give the external observer an advantage. First, we as an observer defined a model of the optical projection neuron response before knowing what the response will look like. Second, again as an observer, we used the alpha function fitted to the entire response to measure at each point in time the instantaneous amplitude and its change. Third, the classification was performed piece-wise by recomputing the discriminant functions for each time bin. Fourth, these discriminant functions were computed only after selecting those subsets of glomeruli that provided the best results. While it is obvious that these techniques prevent us from concluding that the insect brain decodes those same signals using the same methods, it is important to emphasize again that the decoding question is distinct from the encoding question addressed here. Hence, our conclusion that temporal patterns of projection neuron calcium signals contain odor information remains valid and now warrants the question of the decoding of this information by structures downstream from the projection neurons.

Imaging techniques are a standard and well-established recording method in modern neuroscience (Frostig 2002). Imaging has contributed an immense amount of information to the understanding of brain function (Culham and Kanwisher 2001; Logothetis 2003), last but not least also to the encoding of odors in the antennal lobe or the olfactory bulb (Korsching 2002). Several recent studies have investigated encoding principles of projection neurons based on imaging experiments using the same technique as applied in this paper (Sachse and Galizia 2002, 2003; Galán et al. 2004; Carlsson et al. 2005). The technique we employed has the advantage that it allows to simultaneously measure from an identified neuronal population; the projection neurons. By combining this imaging technique with a model-based analysis of the obtained optical signal, we were able to completely quantify its amplitude-time course. This model-based analysis of optical imaging data allowed us to show that the temporal dynamics of calcium as measured optically provide a substantial amount of information beyond what is encoded in spatial activation patterns alone. Hence, it will be interesting to see whether model based analysis methods will provide the means to also extract and quantify in other preparations information contained in the temporal dimension of imaging data.

One important aspect of the imaging technique we employed is that the measured optical signal also depends on the intracellular concentration of the dye. This issue,

however, is irrelevant to our conclusion because we compared in our analysis of the encoding performance only responses of the same glomerulus to different odor stimuli. Hence, all the responses considered have the same dye-induced distortion, and any differences between those responses can only be due to the different stimuli.

In previous studies of related system, it has been shown that the temporal sequence of synchrony across projection neurons is stimulus dependent (Laurent et al. 1996; Wehr and Laurent 1996) and that their desynchronization causes information loss in downstream neurons (MacLeod et al. 1998). Spike counts or instantaneous (and optically measured) response amplitudes of populations of projection neurons or mitral cells were used to show that the discrimination of odor stimuli improves with time (Friedrich and Laurent 2001; Stopfer et al. 2003; Friedrich and Laurent 2004; Galan et al. 2004; Mazor and Laurent 2005). Moreover, stimulus induced temporal modulations of the projection neuron/mitral cell response have been reported for a range of stimulus durations, from 0.1 to 2.4 s (Friedrich and Laurent 2001; Laurent 2002; Stopfer et al. 2003; Friedrich and Laurent 2004; Lei et al. 2004; Carlsson et al. 2005). Such a temporal modulation of projection neuron/mitral cell responses on a hundreds of milliseconds time scale has been reported in various species (Laurent 1996; Friedrich and Laurent 2001; Stopfer et al. 2003; Galán et al. 2004; Mazor and Laurent 2005; Lei et al. 2004; Carlsson et al. 2005). These temporal modulations were found to depend on odor identity and concentration. Thus, the *idea* that these temporal patterns may contain information about odor stimuli exists already for a long time in the literature. However, so far a *proof* of this idea in terms of a quantification of the information content of these temporal patterns has been missing. Here we extended these results by showing that both temporal and spatial components of the optical signal contain odor information. Specifically, we demonstrated that the discrimination of odor stimuli can be more accurate if the instantaneous response amplitudes of the optical responses of a population of projection neurons are combined with a measure of their temporal dynamics. Hence, the temporal patterns of the optical projection neuron response contain information about odor stimuli. In other words, we proved the long-standing idea that these temporal modulations of projection neuron activity, measured on a hundreds of milliseconds time scale, contain information about odor stimuli. This encoding of odor stimuli is distinct from an earlier proposed temporal encoding into sequences of synchronized projection neuron assemblies (Laurent 2002).

In general, our results show that temporal modulations of neuronal activity at a time scale of hundreds of milliseconds contain stimulus-specific information. Such a temporal population code was identified earlier using theoretical means (Wyss et al. 2003a, 2003b; Knüsel et al. 2004). In this article we provide empirical evidence that internally generated dynamics of the nervous system – in our case the antennal lobe – transform static stimulus features in a representation where temporal dynamics of neuronal activity could provide an additional channel to transmit information. On the basis of our results we predict that this transformation of static stimulus features into a representation where temporal patterns contain stimulus-specific information is a generic property of densely laterally coupled neuronal structures. We theoretically investigated this hypothesis in a simulated model of the moth antennal lobe (Knüsel and Verschure 2006) in the paper following this article (Knüsel and Verschure 2006).

Acknowledgments

This work was supported by the EU Future and Emerging Technologies Programme (IST-2001-33066 (AMOTH)).

Appendix A: Optical projection neuron response and its model

Optical projection neuron response

The optical projection neuron response is the bleaching corrected luminance measured from the center of the glomeruli of the antennal lobe. A well-known problem with optical imaging using calcium-sensitive dyes is that the data must be corrected for bleaching. In case of FURA-dextran, this correction must be performed independently for both the 340 nm and 380 nm sequences since the time constant of the bleaching is different (as will be shown subsequently). Here, we correct for bleaching by fitting a function to the fluorescence response of all frames excluding the 30 frames after stimulus onset. Subsequently, these two functions are used to correct all frames in the sequence. We capture the bleaching effect using an exponential

$$B(t_i; A, B, \tau_{\text{bleach}}) = A + B \exp\left(-\frac{t_i}{\tau_{\text{bleach}}}\right) \quad (3)$$

where the fitting parameters are the offset, A , the amplitude, B , and the time constant, τ_{bleach} . For each illumination wavelength, this procedure results in two exponentials, $b_{340}(t_i)$ and $b_{380}(t_i)$ where $\langle \tau_{340} \rangle = 6.9 \pm 3.1$ and $\langle \tau_{380} \rangle = 9.4 \pm 5.9$ (median and halved interquartile range). The bleaching-corrected ratio, F_{ratio} , is computed following

$$F_{\text{ratio}}(t_i, \mathbf{x}) = \frac{F_{\text{raw},340}(t_i, \mathbf{x}) - [b_{340}(t_i) - \min_i b_{340}(t_i)]}{F_{\text{raw},380}(t_i, \mathbf{x}) - [b_{380}(t_i) - \min_i b_{380}(t_i)]} \quad (4)$$

where \mathbf{x} denotes a pixel, and $t_i, i = 1, 2, \dots, 70$ the frame. $F_{\text{raw},340}$ and $F_{\text{raw},380}$ are the raw responses to illumination with 340 nm and 380 nm respectively, and $\min_i(\cdot)$ is the minimum value of the argument over i .

Borders of glomeruli are visible in the fluorescence image and quadratic regions of interest of size 10×10 pixels (about $10 \mu\text{m} \times 10 \mu\text{m}$) are drawn in the centers of the glomeruli. The size of the regions of interest fits well within the size of a glomerulus ($50 \mu\text{m}$) and the position in the center limits light scattering from neighboring glomeruli. Smaller regions render noisier time courses and larger regions do not further improve the signal-to-noise ratio. Subtracting the mean fluorescence before stimulation (frame 2–20) from $F_{\text{ratio}}(t_i, \mathbf{x})$ for each frame, i , and averaging over all pixels, $\mathbf{x} \in S$, of a region of interest, S , yields the *optical projection neuron response*,

$$F_{\text{PN}}(t_i) = \langle F_{\text{ratio}}(t_i, \mathbf{x}) - \langle F_{\text{ratio}}(t_j, \mathbf{x}) \rangle_{j=2, \dots, 20} \rangle_{\mathbf{x} \in S}, \quad (5)$$

where $\langle \cdot \rangle$ denotes the average value over the specified variables and ranges.

Model function of projection neuron response

In order to fit the optical projection neuron response we need a biophysical model that accurately describes the intracellular calcium dynamics due to both stimulus- and dye-dependent effects. Usually, single synaptic calcium input currents are modeled using exponential decays or alpha functions (Dayan and Abbott 2001). Here, however, we need to describe the calcium dynamics that results from many synaptic events over a number of seconds. Our model is based on the assumption that first order kinetics govern the increase of the intracellular calcium concentration in the projection neurons upon odor stimulation (Stetter et al. 2001). In this case, the total ionic calcium input current to a projection neuron is given by an exponential decay

$$I(t) \propto \begin{cases} 0 & \text{if } t < s \\ \exp\left(-\frac{t-s}{\tau_I}\right) & \text{else} \end{cases} \quad (6)$$

where t is time, s denotes stimulus onset, and τ_I is the time constant. If the validation of the model function derived here shows that it provides an accurate description of the optical projection neuron response, this suggests that our assumption of first order kinetics may be correct (see subsequently for a validation of our model). Using single compartment models, the dynamics of the intracellular calcium concentration in the presence of a dye have been described with first-order differential equations (Neher and Augustine 1992; Helmchen et al. 1996), the general solution of which is that the free intracellular calcium concentration is described as the convolution of the input current with an exponential decay (Yasuda et al. 2004). Here, we assume that all processes of the projection neuron that are imaged using FURA-dextran can be considered as one compartment, i.e., influx, efflux, and buffering is uniform throughout. Combining these models of the dynamics of the free intracellular calcium concentration, $[\text{Ca}^{2+}]_i(t)$, with our assumption of an exponentially decaying input current (Equation 6) renders

$$[\text{Ca}^{2+}]_i(t) \propto \exp\left(-\frac{t-s}{\tau_D}\right) - \exp\left(-\frac{t-s}{\tau_I}\right). \quad (7)$$

τ_D is the decay time constant of $[\text{Ca}^{2+}]_i$ to a brief impulse of calcium input current (impulse response), and τ_I is the time constant of the projection neuron input current (Equation 6). Thus, the free intracellular calcium concentration, $[\text{Ca}^{2+}]_i(t)$, is proportional to the difference of two exponentials with time constants τ_D and τ_I .

For $\tau_D \rightarrow \tau_I$, this difference can be approximated by a so-called alpha function (Figure 1 and Appendix C)

$$\alpha(t; S, B, \tau, t_0) = B + \begin{cases} 0 & \text{if } t < t_0 \\ S \frac{t-t_0}{\tau} \exp\left(-\frac{t-t_0}{\tau}\right) & \text{else} \end{cases} \quad (8)$$

if $\tau_D > \tau_I$. In case of $\tau_D < \tau_I$, the difference is $-\alpha(t; S, B, \tau, t_0)$. The four parameters of the alpha function, the amplitude-coefficient, S , the baseline, B , the time constant, τ , and the response onset, t_0 , are found with, for example, nonlinear regression.

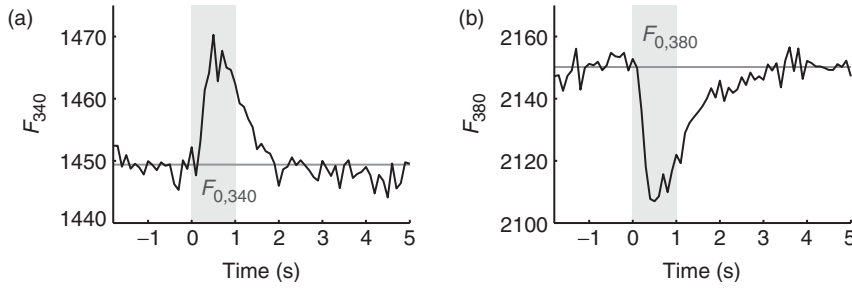


Figure 8. Bleaching-corrected response of an arbitrary glomerulus to geraniol (100 μg) upon illumination of the antennal lobe with light at (a) 340 nm and (b) 380 nm. Note the high background fluorescence ($F_{0,340}$ and $F_{0,380}$), indicated by the grey horizontal line. The shaded area indicates the stimulus.

The fluorescence intensity after bleaching-correction, $\hat{F}(t)$, depends linearly on $[\text{Ca}^{2+}]_i(t)$ if the dissociation constant of FURA-2, K_D , is much smaller than the intracellular calcium concentration, that is, $[\text{Ca}^{2+}]_i(t) \ll K_D$ (Yasuda et al. 2004). Indeed, there is evidence that this assumption is satisfied. In *Drosophila* motor neurons, the intracellular calcium concentration was determined to be about 23 ± 11 nM (Macleod et al. 2002) while the dissociation constant of FURA-2 is around 140 nM (Molecular Probes, Inc., Eugene, OR, USA). Thus, since the bleaching-corrected fluorescence depends linearly on the intracellular calcium concentration, it can be approximated with an alpha function,

$$\hat{F}(t) = \hat{F}_0 + \alpha(t; S, B, \tau, t_0), \quad (9)$$

where \hat{F}_0 is the constant background fluorescence. (We always use the capital letter F for the *measured* fluorescence response whereas the *modeled* fluorescence response will have a hat, \hat{F} .)

We now showed that the fluorescence response can be approximated with an alpha function. In case of FURA-2, the probe is illuminated with two frequencies (340 nm and 380 nm) resulting in two fluorescence responses, one of which has a positive, the other a negative peak (Figure 8) (Grynkiewicz et al. 1985). Thus, with \hat{F}_{340} and \hat{F}_{380} the bleaching-corrected responses at 340 nm and 380 nm, we obtain

$$\hat{F}_{340}(t) = \hat{F}_{0,340} + \alpha_{340}(t; S_{340}, B_{340}, \tau_{340}, t_{0,340}) \quad (10)$$

$$\hat{F}_{380}(t) = \hat{F}_{0,380} - \alpha_{380}(t; S_{380}, B_{380}, \tau_{380}, t_{0,380}) \quad (11)$$

where $\hat{F}_{0,340}$ and $\hat{F}_{0,380}$ are the background fluorescences defined as the mean fluorescence of frames 2–20. The parameters S , B , τ , and t_0 are defined above. Note the minus sign of the 380 nm response which is due to the properties of the dye. The ratio of these sequences is the *modeled* optical projection neuron response, \hat{F}_{PN} ,

$$\hat{F}_{\text{PN}}(t) = \frac{\hat{F}_{340}(t)}{\hat{F}_{380}(t)} \quad (12)$$

$$= \frac{\hat{F}_{0,340} + \alpha_{340}(t)}{\hat{F}_{0,380} - \alpha_{380}(t)}. \quad (13)$$

For simplicity, we omitted the parameters of the alpha function. It is important to note that the average background fluorescence is much greater than the stimulus-evoked change in fluorescence (Figure 8), that is, $\hat{F}_{0,z} \gg \max_t(\alpha_z(t))$, $z \in \{340, 380\}$. Thus, Equation 13 can be approximated by its Taylor series, resulting in (Appendix C)

$$\hat{F}_{\text{PN}}(t) \approx \frac{\hat{F}_{0,340}}{\hat{F}_{0,380}} + \frac{1}{\hat{F}_{0,380}} \alpha_{340}(t) + \frac{\hat{F}_{0,340}}{\hat{F}_{0,380}^2} \alpha_{380}(t). \quad (14)$$

The sum of the two alpha functions in Equation 14 can be replaced by a single alpha function if τ and t_0 are about equal. In order to show that, we note that the dynamics of the fluorescence response to illumination with 340 nm or 380 nm only depend on the odor-evoked fluctuations of the intracellular calcium concentration and not on the illumination wavelength. Therefore, the time constants τ_{340} and τ_{380} and the response onset times t_{340} and t_{380} are approximately equal and the sum of the two alpha functions in Equation 14 simplifies to

$$\hat{F}_{\text{PN}}(t) \approx \frac{\hat{F}_{0,340}}{\hat{F}_{0,380}} + \frac{\hat{F}_{0,340}S_{380} + \hat{F}_{0,380}S_{340}}{\hat{F}_{0,380}^2} \alpha(t; S, B, \tau, t_0) \quad (15)$$

$$= \alpha(t; S \cdot k_2, B + k_1, \tau, t_0). \quad (16)$$

α is an alpha function with an appropriately chosen set of parameters S , B , τ , and t_0 determined with nonlinear regression (Seber and Wild 1989), and $k_1 = \hat{F}_{0,340}/\hat{F}_{0,380}$ and $k_2 = \hat{F}_{0,340}S_{380} + \hat{F}_{0,380}S_{340}/\hat{F}_{0,380}^2$ are two constants. Hence, under the assumption of an exponential calcium influx to the projection neurons of a single glomerulus (Equation 6), this analysis predicts that the *measured* optical projection neuron response, F_{PN} (Equation 5), can be approximated by a single alpha function (Equation 16).

Response amplitude and duration

In our further analysis we only want to consider those parameters of the alpha function that define the temporal dynamics of the response. Hence, out of the four parameters of the alpha function, we focus here on only two of them, the amplitude-coefficient and the time constant, or their linearly dependent counterparts, the projection neuron response amplitude and duration.

The response amplitude, A , is defined as the maximum value of the alpha function minus the baseline shift, B . Since the alpha function is maximal at time $t = t_0 + \tau$ (Figure 1), we have

$$A = \alpha(t_0 + \tau; S, B, t_0, \tau) - B = S \exp(-1) = \frac{S}{e} \quad (17)$$

where $e \approx 2.72$ is the base of the natural logarithm. Thus, the response amplitude equals the amplitude-coefficient of the alpha function, S , divided by e . The response duration, D , is defined as the width of the alpha function at half maximum, that is $(S/2e) + B$ (Figure 1). The width is delimited by two

points in time, t_1 and t_2 , where the alpha function equals $(S/2e) + B$. Thus, t_1 and t_2 have to satisfy

$$\alpha(t_{1/2}; S, B, t_0, \tau) \stackrel{!}{=} \frac{S}{2e} + B \quad (18)$$

$$\Leftrightarrow \frac{t_{1/2} - t_0}{\tau} \exp\left(-\frac{t_{1/2} - t_0}{\tau}\right) \stackrel{!}{=} \frac{1}{2e} \quad (19)$$

$$\Leftrightarrow x_{1/2} \exp(-x_{1/2}) \stackrel{!}{=} \frac{1}{2e} \quad (20)$$

where we set $x_{1/2} := (t_{1/2} - t_0)/\tau$. Equation 20 has two solutions x_1 and x_2 that can be found numerically. The duration is then given by

$$D = t_2 - t_1 = \tau(x_2 - x_1) \approx \tau \cdot 2.45 \quad (21)$$

where τ is the time constant of the alpha function. Thus, the response amplitude only depends on the amplitude-coefficient of the alpha function, and the response duration only depends on its time constant.

Appendix B: Fit validation

Methods

The accuracy of the fits is validated by combining both graphical and analytical methods. Model fits that do not satisfy the analytical conditions are rejected.

In order to assess the accuracy of the fit we use three measures, the adjusted R^2 statistic, the amplitude-to-noise ratio and the t -statistic. The adjusted R^2 statistic, R_{adj}^2 , is based on the sum of squared residuals, S_{err}^2 , and the total sum of squares around the mean, S_{tot}^2 . With $F_i = F_{\text{PN}}(t_i)$ the measured optical projection neuron response and $\hat{F}_i = \hat{F}_{\text{PN}}(t_i)$, $i = 1, 2, \dots, n$ the fitted optical projection neuron response, the sums are expressed as

$$S_{\text{err}}^2 = \sum_{i=2}^n (F_i - \hat{F}_i)^2 \quad (22)$$

$$S_{\text{tot}}^2 = \sum_{i=2}^n (F_i - \langle F \rangle)^2 \quad (23)$$

where $n = 70$ is the number of data points, and $\langle F \rangle$ is the mean of F_i . Then, R_{adj}^2 , which measures the fraction of S_{tot}^2 explained by the function \hat{F}_{PN} is expressed as

$$R_{\text{adj}}^2 = 1 - \frac{S_{\text{err}}^2(n-1)}{S_{\text{tot}}^2(n-p)} \quad (24)$$

where n is the number of data points and p the number of parameters of the model function. The value of R_{adj}^2 is always lower or equal to 1, and a value closer to 1 indicates a better fit.

The second measure, the amplitude-to-noise ratio, compares the response amplitude, A , to the standard deviation of the residuals (noise), σ . According to the assumptions of nonlinear regression (Seber and Wild 1989), the residuals

$$\varepsilon_i \sim F_{\text{PN}}(t_i) - \hat{F}_{\text{PN}}(t_i) \quad (25)$$

are Gaussian with zero mean and variance σ^2 , $\varepsilon_i = \mathcal{N}(0, \sigma^2)$. Thus, we consider the ratio

$$\eta = \frac{A}{\sigma} \quad (26)$$

to test whether η is not from $\mathcal{N}(0, 1)$, the standard normal distribution, at significance level of α . As $A > 0$, we use a one-sided test, that is,

$$\Pr(\eta > \theta) > \alpha \quad (27)$$

defines a threshold, θ , for which η is from $\mathcal{N}(0, 1)$ with probability α . θ can be computed using the cumulative distribution function of the standard normal distribution. For $\eta > \theta$, the response amplitude is significantly larger than a value randomly drawn from the distribution of the residuals, $\mathcal{N}(0, \sigma^2)$. Thus, the projection neuron response cannot be due to random noise in the fluorescence signal with probability $1 - \alpha$.

Finally, we use the t -statistic to verify whether the estimated amplitude-coefficient, S , and the time constant, τ , of the alpha function are significantly different from zero. The t -statistic is defined as the ratio between the estimated parameter value and its standard error where $n = 69$ is the number of data points. At a significance level of 0.05, the estimated values are significantly larger than zero if the ratio is larger than 1.67 (inverse of the Student's cumulative distribution function with $n - 1$ degrees of freedom).

Results

A standard measure to validate fits is the adjusted R^2 statistic, R_{adj}^2 . Generally, this measure suffers from one central problem: neither do large values of R_{adj}^2 guarantee a good fit, nor do low values of R_{adj}^2 allow the conclusion of a bad fit. Thus, verifying fits by only reporting R_{adj}^2 is not enough. Therefore, as a first evaluation of the ability of our model to describe the data, we visually inspect the goodness of the fit for a broad range of R_{adj}^2 -values (Figure 9). We observe that the model follows the optical projection neuron response well for all values of R_{adj}^2 while the prediction bounds are wider for lower values of R_{adj}^2 compared to the other fits (Figure 9, first column). This demonstrates that our alpha function model is valid for a broad range of values of R_{adj}^2 , with lower values corresponding to optical projection neuron responses with lower amplitudes, and, therefore, to fits that are intuitively worse. In order to further validate the sufficiency of our model, we test whether the residuals of the fit follow a normal distribution with constant standard deviation and zero mean. The scatter plots of the residuals vs. the predictor variable time (Figure 9, second column) indeed show a constant standard deviation and zero mean. Finally, projecting the residuals against a normal distribution shows that they fall on a straight line, i.e., they follow a normal distribution (Figure 9, third column). This is further confirmed

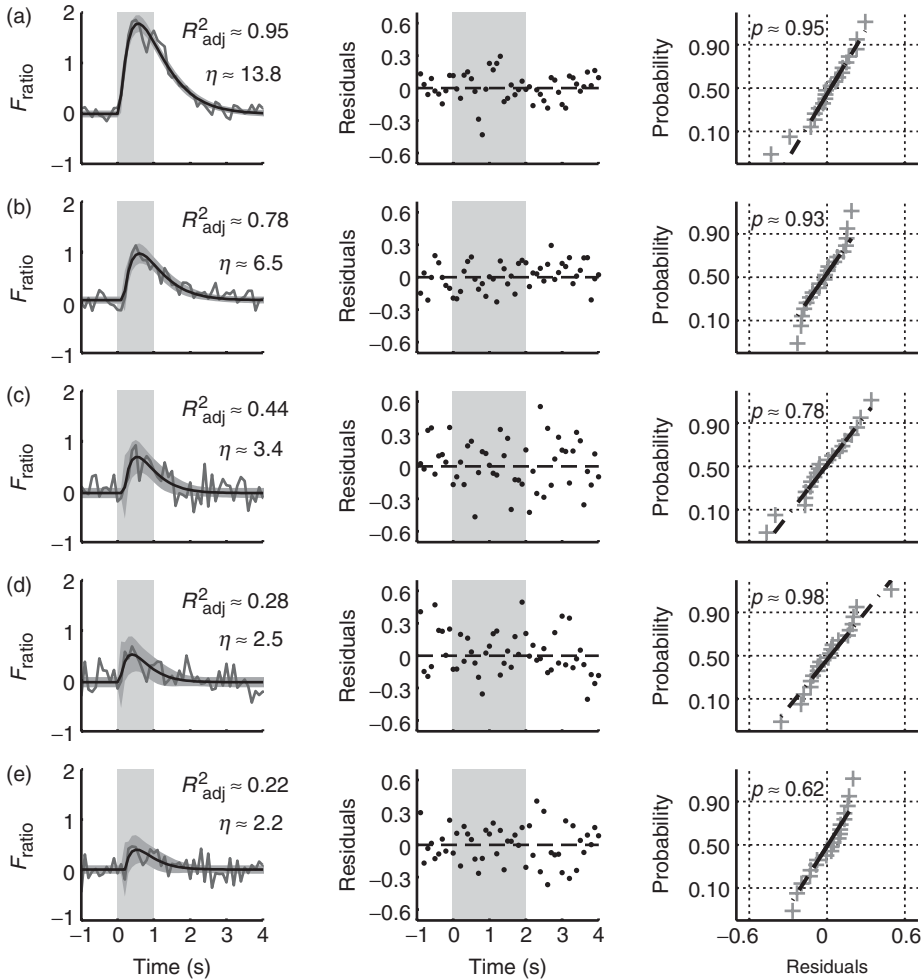


Figure 9. Graphical evaluation of goodness of fit. First column: Fitted alpha function (solid line) including simultaneous prediction bounds (shaded area) overlaid on the optical projection neuron response (dashed line). The grey rectangle indicates the stimulus. Additionally, the adjusted R^2 statistic (R^2_{adj}) and the amplitude-to-noise ratio (η) is given in each plot (“Methods of Appendix B”). Second column: Residuals (dots) computed from the plots in the first column vs. time. The dashed line indicates zero. The grey rectangle indicates the experimental region. Third column: Normal probability plot of the residuals of only the experimental region (grey rectangle in second column) and line joining the first and third quartiles of the residuals (solid line) including an extrapolation out to the extreme values of the residuals (dash-dotted line). The probability value, p , is for testing the hypothesis of a normal distribution of the data (Kolmogorov–Smirnov test). (a–e) Each row shows the same three plots for a different glomerulus with a descending order of R^2_{adj} .

by a statistical test of the goodness-of-fit (Kolmogorov–Smirnov test) of the residuals to a normal distribution (p -values given in Figure 9, third column). In summary, this verification demonstrates that, for a broad range of values of R^2_{adj} , our model fits the optical projection neuron responses well while, in addition, R^2_{adj} scales with the intuitive notion of a good fit.

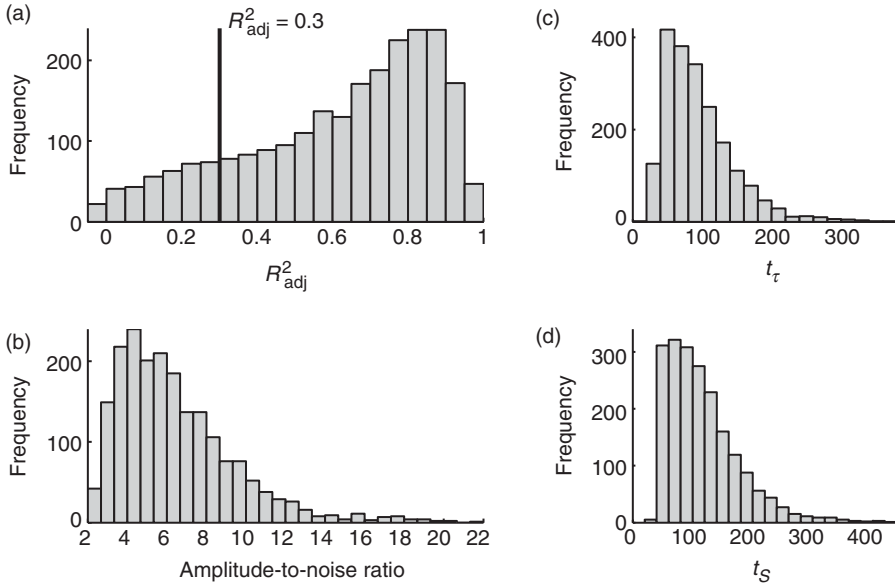


Figure 10. Analytical evaluation of goodness of fit. (a) Distribution of R^2_{adj} for all fits carried out. The vertical black line at 0.3 is the threshold above which fits are accepted. (b) Distribution of the amplitude-to-noise ratio of all fits for which $R^2_{\text{adj}} > 0.3$. The values of the amplitude-to-noise ratio are always larger than 2, corresponding to a significance level of 0.023 (“Methods” of Appendix B). (c,d) t -statistic of the estimated values for the alpha function (c) time constant, τ , and (d) amplitude-coefficient, S . The t -statistic is the estimated parameter value divided by its own standard error. The value of the t -statistic is always larger than 10, corresponding to a significance level of about 2.78×10^{-15} (68 degrees of freedom).

In our further analysis we only want to consider those fits that give a statistically significant value for the amplitude. Hence, we impose a threshold for the R^2_{adj} statistic (Figure 10a). In order to establish this threshold we evaluate the amplitude-to-noise ratio (Figure 10b). We consider an amplitude-to-noise ratio of 2 which gives us a significance level of 0.023. This threshold is equivalent to an R^2_{adj} statistic of 0.3 (i.e., if a fit satisfies $R^2_{\text{adj}} > 0.3$ then $\eta > 2$ is satisfied as well). This procedure results in about 85% of the fits being accepted. Additionally, to confirm that this choice of threshold provides us with a conservative selection of fits, we inspect the t -statistics of the alpha function time constant and amplitude-coefficient (Figure 10c and d). We observe that all values of τ and S are significantly above zero. Thus, this demonstrates that our model provides an accurate description of the optical projection neuron response, that R^2_{adj} is a valid measure to verify fits, and that the chosen threshold is reasonable. Hence, the optical projection neuron response can be accurately described in terms of amplitude and duration.

Appendix C: Mathematical relations

The following shows that the difference of two exponentials can be approximated with an alpha function in the limit of an infinitesimal difference of the

time constants. Consider two exponentials with time constants $\tau_1 > \tau_2$ in the limit of $\tau_1 \rightarrow \tau_2$. Using the series expansion of the exponential function yields

$$b(\tau_1, \tau_2) = \exp\left(-\frac{t}{\tau_1}\right) - \exp\left(-\frac{t}{\tau_2}\right) \quad (28)$$

$$= \sum_{n=0}^{\infty} \frac{1}{n!} \left[\left(-\frac{t}{\tau_1}\right)^n - \left(-\frac{t}{\tau_2}\right)^n \right] \quad (29)$$

$$= \sum_{n=1}^{\infty} \frac{(-t)^n}{n!} \left[\frac{\tau_2^n - \tau_1^n}{(\tau_1 \tau_2)^n} \right] \quad (30)$$

Note that the term for $n=0$ is zero and therefore the sum starts at 1. The term in the square brackets of Equation 30 can be approximated by setting $x := \tau_2 - \tau_1$ and computing its Taylor series around $x_0 = 0$ for $n = 1, \dots, \infty$,

$$d_n(x) = \frac{(\tau_1 + x)^n - \tau_1^n}{\tau_1^n (\tau_1 + x)^n} \quad (31)$$

$$\approx \frac{n}{\tau_1^{n+1}} x \quad (32)$$

$$= \frac{n}{\tau_1^{n+1}} (\tau_2 - \tau_1). \quad (33)$$

Substituting this in Equation 30 yields

$$b(\tau_1, \tau_2) \approx \sum_{n=1}^{\infty} \frac{(-t)^n}{n!} \frac{n(\tau_2 - \tau_1)}{\tau_1^{n+1}} \quad (34)$$

$$\stackrel{m=n-1}{=} \frac{t(\tau_1 - \tau_2)}{\tau_1^2} \sum_{m=0}^{\infty} \frac{1}{m!} \left(-\frac{t}{\tau_1}\right)^m \quad (35)$$

$$= \frac{t(\tau_1 - \tau_2)}{\tau_1^2} \exp\left(-\frac{t}{\tau_1}\right) \quad (36)$$

Thus, in the limit of $\tau_1 \rightarrow \tau_2$, $\tau_1 > \tau_2$, the difference of the two exponentials is an alpha function. It can easily be shown that for $\tau_1 \rightarrow \tau_2$, and $\tau_1 < \tau_2$ the difference is an alpha function multiplied by minus 1.

Finally, we subsequently use the Taylor series expansion to simplify

$$h(x, y) = \frac{A + x}{B - y} \quad (37)$$

in the case of $x \ll A$, $x \ll B$, $y \ll A$, and $y \ll B$. The Taylor series of $h(x, y)$ around $(x_0, y_0) = (0, 0)$ is

$$h(x, y) \approx h(x_0, y_0) + \frac{\partial h(x_0, y_0)}{\partial x} (x - x_0) + \frac{\partial h(x_0, y_0)}{\partial y} (y - y_0) + \dots \quad (38)$$

$$\approx \frac{A}{B} + \frac{1}{B} x + \frac{A}{B^2} y. \quad (39)$$

Thus, for values of x and y that are small compared to A and B , the ratio 37 can be approximated by Equation 39.

References

- Anderson P, Hilker M, Hansson B, Bombosch S, Klein B, Schildknecht H. 1993. Oviposition deterring components in larval frass of *Spodoptera littoralis* (Boisd.) (Lepidoptera: Noctuidae): A behavioural and electrophysiological evaluation. *J Insect Physiol* 39:129–37.
- Anton S, Hansson B. 1994. Central processing of sex pheromone, host odour, and oviposition deterrent information by interneurons in the antennal lobe of female *Spodoptera littoralis* (Lepidoptera: Noctuidae). *J Comp Neurol* 350:199–214.
- Anton S, Hansson B. 1995. Sex pheromone and plant-associated odour processing in antennal lobe interneurons of male *Spodoptera littoralis* (Lepidoptera: Noctuidae). *J Comp Physiol A* 176:773–89.
- Anton S, Homberg U. 1999. Antennal lobe structure. In: Hansson B, editor. *Insect olfaction*. Berlin; *In vivo* optical imaging: London: Springer. pp 97–124.
- Brown S, Joseph J, Stopfer M. 2005. Encoding a temporally structured stimulus with a temporally structured neural representation. *Nat Neurosci* 8:1568–76.
- Carlsson M, Knüsel P, Verschure P, Hansson B. 2005. Spatio-temporal Ca^{2+} dynamics of moth olfactory projection neurons. *Eur J Neurosci* 22:647–57.
- Chapak S, Mertz J, Beaurepaire E, Moreaux L, Delaney K. 2001. Odor-evoked calcium signals in dendrites of rat mitral cells. *Proc Natl Acad Sci USA* 98:1230–4.
- Christensen T, Hildebrand J. 1987. Male-specific, sex pheromone-selective projection neurons in the antennal lobes of the moth *Manduca sexta*. *J Comp Physiol A* 160:553–69.
- Culham J, Kanwisher N. 2001. Neuroimaging of cognitive functions in human parietal cortex. *Curr Opin Neurobiol* 11:157–63.
- Dayan P, Abbott L. 2001. *Theoretical neuroscience: Computational and mathematical modeling of neural systems*. Cambridge, Massachusetts: The MIT Press.
- deCharms R, Zador A. 2000. Neural representation and the cortical code. *Annu Rev Neurosci* 23:613–47.
- Di Lorenzo P, Victor J. 2003. Taste response variability and temporal coding in the nucleus of the solitary tract of the rat. *J Neurophysiol* 90:1418–31.
- Friedrich R, Laurent G. 2001. Dynamic optimization of odor representation by slow temporal patterning of mitral cell activity. *Science* 291:889–94.
- Friedrich R, Laurent G. 2004. Dynamics of olfactory bulb input and output activity during odor stimulation in zebrafish. *J Neurophysiol* 91:2658–69.
- Frostig R, editor. (2002). *In vivo* optical imaging of brain function. CRC Press LLC.
- Galán RF, Sachse S, Galizia C, Herz A. 2004. Odor-driven attractor dynamics in the antennal lobe allow for simple and rapid olfactory pattern classification. *Neural Comput* 16:999–1012.
- Galizia C, Kimmerle B. 2004. Physiological and morphological characterization of honeybee olfactory neurons combining electrophysiology, calcium imaging and confocal microscopy. *J Comp Physiol A* 190:21–38.
- Grynkiewicz G, Poenie M, Tsien R. 1985. A new generation of Ca^{2+} indicators with greatly improved fluorescence properties. *J Biol Chem* 260:3440–50.
- Helmchen F, Imoto K, Sakmann B. 1996. Ca^{2+} buffering and action potential-evoked Ca^{2+} signaling in dendrites of pyramidal neurons. *Biophys J* 70:1069–81.
- Hinks C, Byers J. 1976. *Biosystematics of the genus Euxoa* (Lepidoptera: Noctuidae). V. Rearing procedures and life cycles of 36 species. *Can Entomol* 108:1345–57.
- Jönsson M, Anderson P. 1999. Electrophysiological response to herbivore-induced host plant volatiles in the moth *Spodoptera littoralis*. *Physiol Entomol* 24:377–85.
- Katz D, Simon S, Nicolelis M. 2001. Dynamic and multimodal responses of gustatory cortical neurons in awake rats. *J Neurosci* 21:4478–89.
- Knüsel P, Verschure P. (2006). A model of network mechanisms for decorrelation and complementary encoding in the moth antennal lobe. Submitted.
- Knüsel P, Wyss R, König P, Verschure P. 2004. Decoding a temporal population code. *Neural Comput* 16:2079–100.
- Korsching S. 2002. Olfactory maps and odor images. *Curr Opin Neurobiol* 12:387–92.
- Laurent G. 1996. Dynamical representation of odors by oscillating and evolving neural assemblies. *Trends Neurosci* 19:489–96.
- Laurent G. 2002. Olfactory network dynamics and the coding of multidimensional signals. *Nat Rev Neurosci* 3:884–95.

- Laurent G, Wehr M, Davidowitz H. 1996. Temporal representations of odors in an olfactory network. *J Neurosci* 16:3837–47.
- Lei H, Christensen T, Hildebrand J. 2004. Spatial and temporal organization of ensemble representations for different odor classes in the moth antennal lobe. *J Neurosci* 24:11108–19.
- Logothetis N. 2003. MR imaging in the non-human primate: Studies of function and of dynamic connectivity. *Curr Opin Neurobiol* 13:630–42.
- Macleod G, Hegström-Wojtowicz M, Charlton M, Atwood H. 2002. Fast calcium signals in *Drosophila* motor neuron terminals. *J Neurophysiol* 88:2659–63.
- MacLeod K, Bäcker A, Laurent G. 1998. Who reads temporal information contained across synchronized and oscillatory spike trains? *Nature* 395:693–8.
- Mazor O, Laurent G. 2005. Transient dynamics versus fixed points in odor representations by locust antennal lobe projection neurons. *Neuron* 48:661–73.
- McClurkin J, Optican L, Richmond B, Gawne T. 1991. Concurrent processing and complexity of temporally encoded neuronal messages in visual perception. *Science* 253:675–7.
- Meijerink J, Carlsson M, Hansson B. 2003. Spatial representation of odorant structure in the moth antennal lobe: A study of structure-response relationships at low doses. *J Comp Neurol* 467:11–21.
- Middlebrooks J, Clock A, Xu L, Green D. 1994. A panoramic code for sound location by cortical neurons. *Science* 264:842–4.
- Milner P. 1974. A model for visual shape recognition. *Psychol Rev* 81:521–35.
- Neher E, Augustine G. 1992. Calcium gradients and buffers in bovine chromaffin cells. *J Physiol* 450:273–301.
- Panzeri S, Petersen R, Schultz S, Lebedev M, Diamond M. 2001. The role of spike timing in the coding of stimulus location in rat somatosensory cortex. *Neuron* 29:769–77.
- Ritz R, Sejnowski T. 1997. Synchronous oscillatory activity in sensory systems: New vistas on mechanisms. *Curr Opin Neurobiol* 7:536–46.
- Sachse S, Galizia C. 2002. Role of inhibition for temporal and spatial odor representation in olfactory output neurons: A calcium imaging study. *J Neurophysiol* 87:1106–17.
- Sachse S, Galizia C. 2003. The coding of odour-intensity in the honeybee antennal lobe: Local computation optimizes odour representation. *Eur J Neurosci* 18:2119–32.
- Sadek M, Hansson B, Rospars J, Anton S. 2002. Glomerular representation of plant volatiles and sex pheromone components in the antennal lobe of the female *Spodoptera littoralis*. *J Exp Biol* 205:1363–76.
- Seber G, Wild C. 1989. *Nonlinear regression*. New York: Wiley.
- Singer W, Gray C. 1995. Visual feature integration and the temporal correlation hypothesis. *Annu Rev Neurosci* 18:555–86.
- Sornborger A, Sailstad C, Kaplan E, Sirovich L. 2003. Spatiotemporal analysis of optical imaging data. *Neuroimage* 18:610–21.
- Stetter M, Greve H, Galizia C, Obermayer K. 2001. Analysis of calcium imaging signals from the honeybee brain by nonlinear models. *Neuroimage* 13:119–28.
- Stopfer M, Jayaraman V, Laurent G. 2003. Intensity versus identity coding in an olfactory system. *Neuron* 39:991–1004.
- Von der Malsburg C. (1981). The correlation theory of brain function. MPI Biophysical Chemistry, Internal Report 81-2 reprinted. In Domany E, van Hemmen J, and Schulden K, editors. *Models of Neural Networks II*, 1994. Berlin: Springer.
- Wehr M, Laurent G. 1996. Odour encoding by temporal sequences of firing in oscillating neural assemblies. *Nature* 384:162–66.
- Wyss R, König P, Verschure P. 2003a. Invariant representations of visual patterns in a temporal population code. *Proc Natl Acad Sci USA* 100:324–29.
- Wyss R, Verschure P, König P. 2003b. Properties of a temporal population code. *Rev Neurosci* 14:21–33.
- Yaksi E, Friedrich R. 2006. Reconstruction of firing rate changes across neuronal populations by temporally deconvolved Ca^{2+} imaging. *Nat Methods* 3:377–83.
- Yasuda R, Nimchinsky E, Scheuss V, Pologruto T, Oertner T, Sabatini B, Svoboda K. 2004. Imaging calcium concentration dynamics in small neuronal compartments. *Sci STKE* 2004:pl5.